AFRL-RZ-WP-TP-2010-2056

PLANAR LASER-INDUCED FLUORESCENCE IMAGING OF OH IN A SUPERSONIC COMBUSTOR FUELED WITH ETHYLENE AND METHANE (POSTPRINT)

Campbell D. Carter and Mark R. Gruber

Propulsion Sciences Branch
Aerospace Propulsion Division

Michael D. Ryan

Universal Technology Corporation

Tarun Mathur

Innovative Scientific Solutions, Inc.

FEBRUARY 2010

Approved for public release; distribution unlimited.
See additional restrictions described on inside pages

STINFO COPY

AIR FORCE RESEARCH LABORATORY
PROPULSION DIRECTORATE
WRIGHT-PATTERSON AIR FORCE BASE, OH 45433-7251
AIR FORCE MATERIEL COMMAND
UNITED STATES AIR FORCE

REPORT DOCUMENTATION PAGE

Form Approved
OMB No. 0704-0188

1. REPORT DATE *(DD-MM-YY)*	2. REPORT TYPE	3. DATES COVERED *(From - To)*
February 2010	Journal Article Postprint	10 July 2007 – 10 September 2008

4. TITLE AND SUBTITLE
PLANAR LASER-INDUCED FLUORESCENCE IMAGING OF OH IN A SUPERSONIC COMBUSTOR FUELED WITH ETHYLENE AND METHANE (POSTPRINT)

5a. CONTRACT NUMBER
In-house

5b. GRANT NUMBER

5c. PROGRAM ELEMENT NUMBER
61102F

6. AUTHOR(S)
Campbell D. Carter and Mark R. Gruber (AFRL/RZAS)
Michael D. Ryan (Universal Technology Corporation)
T. Mathur (Innovative Scientific Solutions, Inc.)

5d. PROJECT NUMBER
2308

5e. TASK NUMBER
AI

5f. WORK UNIT NUMBER
2308AI00

7. PERFORMING ORGANIZATION NAME(S) AND ADDRESS(ES)
Propulsion Sciences Branch (AFRL/RZAS)
Aerospace Propulsion Division
Air Force Research Laboratory, Propulsion Directorate
Wright-Patterson Air Force Base, OH 45433-7251
Air Force Materiel Command, United States Air Force

Universal Technology Corporation
Dayton, OH 45432

Innovative Scientific Solutions, Inc.
Dayton, OH 45440

8. PERFORMING ORGANIZATION REPORT NUMBER
AFRL-RZ-WP-TP-2010-2056

9. SPONSORING/MONITORING AGENCY NAME(S) AND ADDRESS(ES)
Air Force Research Laboratory
Propulsion Directorate
Wright-Patterson Air Force Base, OH 45433-7251
Air Force Materiel Command
United States Air Force

10. SPONSORING/MONITORING AGENCY ACRONYM(S)
AFRL/RZAS

11. SPONSORING/MONITORING AGENCY REPORT NUMBER(S)
AFRL-RZ-WP-TP-2010-2056

12. DISTRIBUTION/AVAILABILITY STATEMENT
Approved for public release; distribution unlimited.

13. SUPPLEMENTARY NOTES
Journal article published in *Proceedings of the Combustion Institute*, Vol. 32 (2009). Paper contains color. PA Case Number: 88ABW-2007-0649; Clearance Date: 06 Dec 2007. © 2009 Published by Elsevier Inc. on behalf of The Combustion Institute. The U.S. Government is joint author of this work and has the right to use, modify, reproduce, release, perform, display, or disclose the work.

14. ABSTRACT
A supersonic combustor was experimentally investigated using both conventional instrumentation and laser-based diagnostics. Planar laser-induced fluorescence (PLIF) imaging of OH was used in the main section of the combustor to examine flameholding and flame propagation during a series of evaluations at conditions simulating Mach-5.5 flight. Parameters of interest in this study included the angle of the primary fuel injectors, the distribution of fuel throughout the combustor, and the fuel composition. Changes in fuel injection angle were expected to influence the mixing and combustion processes, and therefore combustor operation. Fuel-distribution variations were expected to modify the flame propagation between flameholding regions. Finally, ethylene and methane were used to examine the suitability of the flameholder designs over a wide range of fuel reactivity. Results suggest that the combustor provides relatively robust flameholding regardless of the fuel used and good flame propagation as long as the fuel distribution provides favorable conditions in the flameholding regions.

15. SUBJECT TERMS
Scramjet, Supersonic combustion, OH PLIF, Combustor performance, Flameholding

16. SECURITY CLASSIFICATION OF:			17. LIMITATION OF ABSTRACT:	18. NUMBER OF PAGES	19a. NAME OF RESPONSIBLE PERSON (Monitor)
a. REPORT	b. ABSTRACT	c. THIS PAGE			Campbell D. Carter
Unclassified	Unclassified	Unclassified	SAR	14	19b. TELEPHONE NUMBER *(Include Area Code)* N/A

Standard Form 298 (Rev. 8-98)
Prescribed by ANSI Std. Z39-18

Available online at www.sciencedirect.com
ScienceDirect
Proceedings of the Combustion Institute 32 (2009) 2429–2436
Proceedings of the Combustion Institute
www.elsevier.com/locate/proci

Planar laser-induced fluorescence imaging of OH in a supersonic combustor fueled with ethylene and methane

Michael Ryan [a,*], Mark Gruber [b], Campbell Carter [b], Tarun Mathur [c]

[a] Universal Technology Corporation, Dayton, OH 45432, USA
[b] Air Force Research Laboratory, Wright Patterson AFB, OH 45433, USA
[c] Innovative Scientific Solutions, Inc., Dayton, OH 45440, USA

Abstract

A supersonic combustor was experimentally investigated using both conventional instrumentation and laser-based diagnostics. Planar laser-induced fluorescence (PLIF) imaging of OH was used in the main section of the combustor to examine flameholding and flame propagation during a series of evaluations at conditions simulating Mach-5.5 flight. Parameters of interest in this study included the angle of the primary fuel injectors, the distribution of fuel throughout the combustor, and the fuel composition. Changes in fuel-injection angle were expected to influence the mixing and combustion processes, and therefore combustor operation. Fuel-distribution variations were expected to modify the flame propagation between flameholding regions. Finally, ethylene and methane were used to examine the suitability of the flameholder designs over a wide range of fuel reactivity. Results suggest that the combustor provides relatively robust flameholding regardless of the fuel used and good flame propagation as long as the fuel distribution provides favorable conditions in the flameholding regions. In addition, the results show that the primary injectors can be useful in controlling certain aspects of combustor operability.

Keywords: Scramjet; Supersonic combustion; OH PLIF; Combustor performance; Flameholding

1. Introduction

Scramjet engines provide the possibility of airbreathing hypersonic flight. To maximize thrust, these engines must be designed to provide adequate mixing and combustion over a short flow path to overcome drag and to minimize structure weight. This is a significant challenge because the residence time inside the combustor is on the order of 1 ms. A common design mechanism involves anchoring flames in lower velocity regions, behind flow obstructions or steps, and in wall cavities to enable the flame to stabilize and burn without blowing off [1]. As the main flow interacts with these recirculation regions across shear layers, the majority of the fuel–air mixture is ignited and burns as it propagates through the combustor.

This work continues the experimental program on scramjet combustors in research cell 22 at the

* Corresponding author. Address: Pratt & Whitney Rocketdyne - West Palm Beach, MS 715-83, PO Box 109600, West Palm Beach, FL 33410-9600.
E-mail addresses: Michael.Ryan3@wpafb.af.mil, Michael.Ryan@pwr.utc.com (M. Ryan).

1540-7489/$ - see front matter © 2009 Published by Elsevier Inc. on behalf of The Combustion Institute.
doi:10.1016/j.proci.2008.06.209

Air Force Research Laboratory (AFRL). Goals for this experiment were several, including a better understanding of the role of body and cowl walls on the combustion zone, observation of the influences of fuel reactivity (via changes in fuel composition) on scramjet operation and performance, and an understanding of the effects of primary-fuel-injection angle on combustor performance and operability. This study extends previous work to include the role of body-to-cowl coupling (i.e., body and cowl-side fuel injection and flameholding) at higher Mach numbers and with different fuels.

There are many possibilities for fueling [2–4] and flameholding [5–8] schemes inside these combustors. For this experiment, the combustor was operated with both ethylene and methane as fuels. Ethylene and methane were selected because they essentially bound the entire range of hydrocarbon-fuel reactivity (based on ignition delay time or extinction strain rate) [9,10]. Injection and flameholding/combustor geometry were chosen for performance reasons. The injection scheme for this study is direct-wall injection through an array of ports along the combustor (Fig. 1). This provides more mixing with the main flow than injection inside a cavity, with a lower pressure loss than that of injection behind a strut. To provide improved mixing with the air supply, multiple small injection ports span the width of the combustor. Three flameholding regions are designed into the combustor, with fuel injection ports selectable both upstream and downstream of the main flameholding cavity on the *body-side* wall, and just upstream of the step on the *cowl-side* wall. By varying fuel flow rate, injection angle, injection placement, and fuel choice, observations can be made on the effects of these parameters on the viability and performance of this combustor design.

Ground-based tests of scramjet combustors normally rely on global measurements, such as thrust (via thrust stand) and total heat release (via calorimetry), and wall-based sensors, such as thermocouples and pressure transducers, to determine performance and operability [11,12]. Concurrent hydroxyl (OH) planar laser-induced fluorescence (PLIF) imaging provides the additional ability to examine instantaneous and averaged flame structure at specific positions along the combustor. This adds insight into the specific flow-field and reaction zone that result from changing fuel schemes and combustor geometries.

PLIF of the OH radical is a well-established technique for study of the reaction zone in a turbulent, non-premixed flame [13]. Its tendency to persist downstream of the flame front at super-equilibrium concentrations, especially in premixed flames, limits one in discerning between the reaction zone and hot combustion products. However, the OH signal can be used as a reaction progress variable for a specific performance metric and also in general to gain insight into the combustion dynamics of supersonic combustors [14–17].

2. Experimental apparatus

2.1. Facility

The direct-connect supersonic combustion facility at AFRL [18–20] is continuously supplied with clean air up to 13.6 kg/s at 5.2 MPa and 920 K total pressure and temperature. A hydrocarbon-fueled vitiator can further heat the supply air to 2500 K. The entire combustor is mounted on a thrust stand to measure thrust. In addition the facility is instrumented with multiple pressure taps and thermocouples for evaluating combustor performance. Combustor run times are typically 30 s to limit heat load to certain combustor components. For this study a 2D Mach-2.84 facility nozzle and a distortion generator [21] were installed to simulate an engine at Mach-5.5 flight speed. The air was supplied at 4.2 kg/s and had stagnation conditions of 1388 K and 1.7 MPa.

Within the combustor a flameholding cavity on the *body* (top) *side* is recessed from the surface with a 90° upstream facing step and a 22.5° trailing edge ramp (see Fig. 1). The cavity has a depth of 2.2 cm. and a length of 7.1 cm. Fuel-injection ports are placed upstream and downstream of the cavity as well as on the *cowl* (bottom) *side* of the combustor at the cavity. B1 and B2 denote

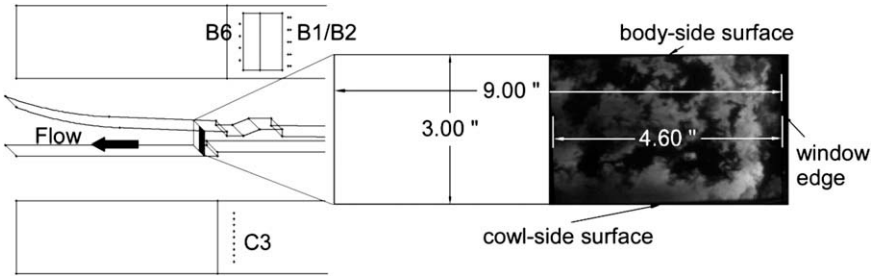

Fig. 1. Combustor geometry showing image plane. Image is taken from run A.

inclined (30°) and normal injectors, respectively, of which there are five, each separated by 3.8 cm. There are four B6 fuel ports normal to the wall, also 3.8 cm apart, and nine normal C3 ports, 2 cm apart. Flameholding expansion steps are placed downstream of the cavity for both the body and cowl side of the combustor. The body-side step is 1.2 cm deep, spanning the width of the tunnel, and is located 5.1 cm downstream of the edge of the cavity ramp. The cowl-side step is 1.3 cm deep and is located 8.1 cm downstream of the cavity. A 36-cm-long quartz window is placed on one side of the combustor downstream of the cavity to allow both laser and camera-viewing access for the OH PLIF through its entire 7.6-cm height. Both fuels are at least 98% pure; additionally, while the ethylene was injected near 300 K, the methane was preheated to 590 K. Ethylene was injected at room temperature because it requires no additional heating to improve its reactivity in the current flow environment. Unheated methane, however, did not produce sustainable flames. The preheat temperature of 590 K is a practical limit for fuel heater operation and was approximately the minimum value required for sustainable flames.

2.2. OH planar laser induced fluorescence

The OH PLIF set-up is shown in Fig. 2. The second harmonic of a 10-Hz Spectra Physics GCR-170 Nd:YAG laser was used to pump a Lumonics Hyperdye dye laser. The resulting dye laser beam was then frequency doubled using an Inrad Autotracker III to produce ~10 mJ/pulse at 283.5 nm. The doubled 567 nm dye beam matched the wavelength for the $Q_1(8)$ transition of the $A^2\Sigma^+ \leftarrow X^2\Pi$ ($v' = 1, v'' = 0$) band of OH. The pump transition was a compromise between reasonable signal and insensitivity to temperature change. The desired pump beam was separated from the fundamental dye beam by way of a prismatic harmonic separator. A small portion of the beam was directed over a reference flame and then to a fast photodiode by way of a fused-silica flat to enable constant monitoring of laser tuning and pulse energy. The sheet was formed by first sending the beam through a −5 cm focal length plano-concave fused silica lens then through a 1 m focal length biconvex spherical fused silica lens; this telescope provided a well-expanded laser sheet that was reasonably uniform in irradiance over the entire combustor height. Limited optical access to the combustor resulted in sending the beam through the same window through which the camera viewed the fluorescence. The focusing lens and final turning mirror were located on a translation table as was the camera, enabling translation of the probe region; however, for these measurements the probe plane location was maintained at 5.7 cm downstream of the cowl-side step.

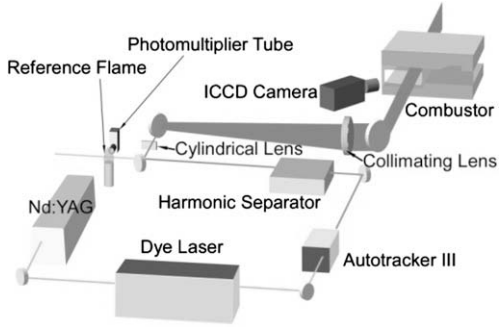

Fig. 2. OH PLIF set-up.

The camera was a Roper Scientific PI-Max intensified CCD camera (512 × 512 pixel array) with a Superblue photocathode; the pixels were binned 2 × 2 before readout so that the camera could achieve a 10 frames/s readout, thus matching the laser repetition rate. The intensifier was gated to 100 ns for each exposure; additionally, the intensifier's micro-channel plate was gated to further reduce the strong flame emission. The Cerco 45-mm focal length, *f*/1.8 UV lens was placed on a Scheimpflug mount so that the laser sheet throughout the depth of the combustor was focused. UG5 and WG305 Schott glass filters were placed on the lens to allow detection of the A–X ($v' = 1, v'' = 1$) and (0,0) band fluorescence – where the $v' = 0$ level is populated through vibrational energy transfer – while blocking laser scattering, (1,0) band fluorescence, and background flame luminosity. Because of the limited optical access, the camera was only able to view the half of the combustor closest to the window. A representative OH PLIF image with the flowpath geometry is shown in Fig. 1. A series of 200 images was taken for each fueling condition, after combustion had reached a steady state. The first 20 images of that sequence were taken with the laser shuttered off for background luminosity subtraction. The images were *de-warped*, i.e., corrected for perspective distortion, using a projective transformation after determining the field of view by imaging a grid of dots at the laser plane.

3. Results

The fueling parameters of the runs to be discussed are shown in Table 1. This is a representative group that shows the general trends in the data. A broad test matrix was explored (including various fuel mixtures between ethylene and methane) but for brevity, only certain cases were selected for inclusion in this paper. Uncertainties for combustor fuel flow rate and equivalence ratio are ±0.6% and ±2.5% of reading, respectively. The effect of primary-injector angle was compared

Table 1
Fueling parameters used for OH PLIF imaging

Run	Fuel	Total Φ	Fuel distribution (%)			
			B1	B2	B6	C3
A	Ethylene	0.80	49		25	26
B	Ethylene	0.68	42		29	30
C	Ethylene	0.40		100		
D	Ethylene	0.81		50	24	26
E	Ethylene	0.69		43	27	29
F	Methane	0.79		49	25	26

directly using cases A and D (at high overall ϕ and high percentage from the primary injectors) and cases B and E (at lower overall ϕ and lower percentage from the primary injectors). The influence of fuel composition is compared in cases D and F. The influence of adding secondary fuel is observed by comparing cases C and D.

3.1. OH PLIF imaging

Sample instantaneous, de-warped PLIF images can be seen in Figs. 3 and 4, from runs D and F, respectively. Note that the laser sheet is not square because there is a lip on the bottom of the window and the sheet is tilted slightly downwards. These images are characteristic of most images taken for this study. There is a large range of scales seen in the fluid structures that contain OH. When fueled on the cowl side, there is a large region near the bottom wall of the combustor that contains the flame or combustion products. The region just above this typically has intermittent smaller structures propagating through it. At the top of the images, the probability of finding OH depends on where the body side is fueled; for example, the probability is lower directly downstream of the B6 injectors. The turbulent nature of the flow exhibits itself by the convoluted edges of the flow structures containing OH.

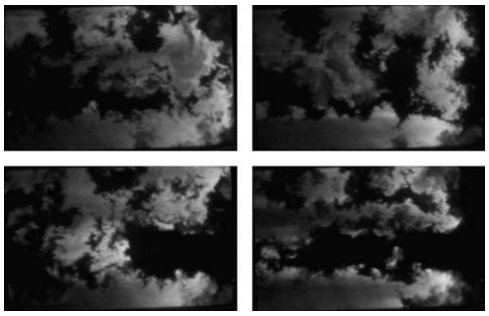

Fig. 3. Individual images from run D.

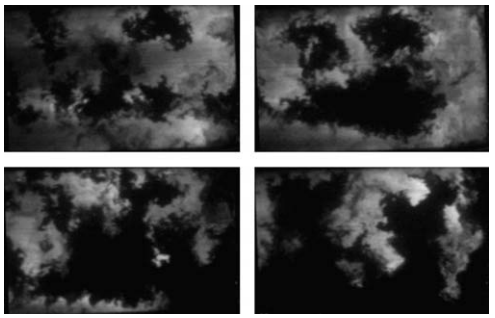

Fig. 4. Individual images from run F.

Of course, OH on the right side of the image absorbs laser energy, thereby decreasing the signal on the left side. Also, the left side of the image is more strongly affected by fluorescence trapping. The path length of the fluorescence from the left side of the image through the combustor to the detector is 20–30 cm. An additional problem with signal consistency from run to run is slight abrasion of the inside window surface during each run, blurring the image and potentially distorting the laser sheet. For this particular set of measurements, the window was replaced just once, after the surface polish had degraded beyond an acceptable level.

Statistical images were compiled for each run, with the average signal, $\overline{S}_{\mathrm{LIF}}$, and standard deviation divided by average signal, $\widehat{\sigma} \equiv \sigma/\overline{S}_{\mathrm{LIF}}$, being calculated. All of these images are displayed in Fig. 5, with the average image on the left of the corresponding scaled-standard-deviation image in each pairing. Because of the significant absorption of both laser energy and fluorescence signal, the intensities of OH detected by the camera are not uniform across the image. Normalizing the standard deviation images helps account for the lower average signal on the left side of the image. However, this approach can create artifacts of low values where the average fluorescence intensity is high.

With cowl-side fueling (all runs except C), there is a large average amount of OH at the floor of the combustor. This shows the burning local to the cowl side as the mixed fuel and air propagate over the flame that is sustained in the recirculation region behind the step. The laser sheet location, 5.7 cm downstream of the cowl-side step, is downstream of this recirculation region. The dark region directly above this is the edge of that burning region; of course, the exact location of this boundary fluctuates, leading to an increase in $\widehat{\sigma}$. At the top of the average images, near the body-side surface, $\overline{S}_{\mathrm{LIF}}$ oscillates from light to dark across the image. The dark regions indicate the presence of the fuel-rich plume behind the B6 injectors. However, when fuel is supplied only at B2, as in run C, the OH is more uniform across this region. This pattern can also be seen for the cowl-side injectors, although it is less distinct, since the injectors are smaller and further upstream relative to the image plane.

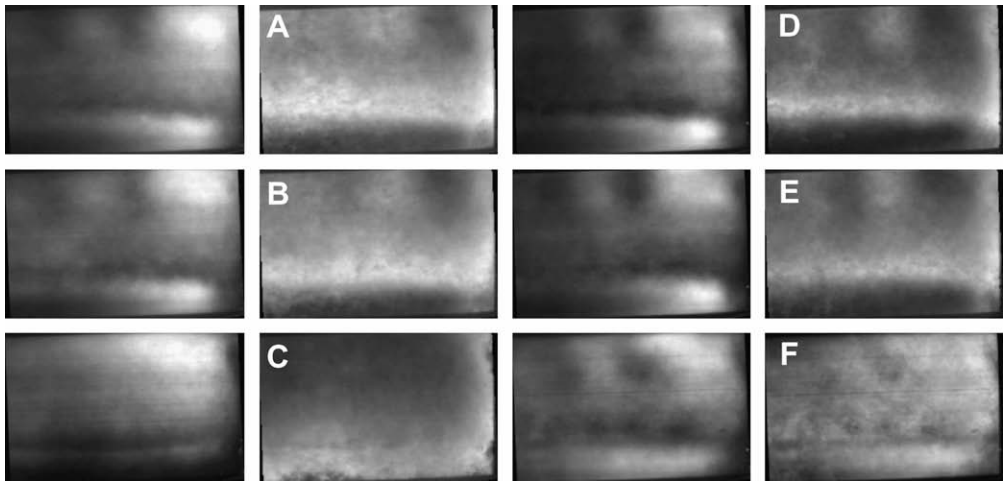

Fig. 5. Mean and scaled-standard-deviation images (left and right, respectively) for each run described in Table 1.

In between the body and cowl wall regions, there is a much lower $\overline{S}_{\mathrm{LIF}}$ and a much larger $\widehat{\sigma}$ directly above the cowl-side flame, indicating that combustion is less likely to be found in this region. Above this, but below the fluid associated with the body-side injectors, there seems to be very little structure in the $\overline{S}_{\mathrm{LIF}}$, along with relatively constant values of $\widehat{\sigma}$.

The flame spreading observations are different when fuel is only supplied at B2 (run C). There is a line of slightly higher OH fluorescence on the cowl side, but this is probably due to the recompression shock behind the cowl-side step. Above this line there is gradually increasing OH signal to the top wall. $\overline{S}_{\mathrm{LIF}}$ decreases across the duct from right to left, which is consistent with a relatively constant average OH number density where fluorescence signal is reduced by laser absorption and fluorescence trapping. In this same region $\widehat{\sigma}$ is relatively constant, except at the window (side wall). This indicates that turbulent mixing carries the fuel across the entire span on average, and transports it with a decreasing degree downwards to the cowl-side wall. $\overline{S}_{\mathrm{LIF}}$ values are slightly lower for this case than cases where fuel is injected through B6 and C3.

When changing the angle of the main fuel injectors from 30° to 90° while keeping the fuel flow rate constant, between cases A → D and B → E, very little difference is observed in the PLIF images. Images of $\overline{S}_{\mathrm{LIF}}$ and $\widehat{\sigma}$ include the same structures with similar sizes. It is possible that the values are slightly different, but because the pump fluence for OH fluorescence depends on the window quality and laser-beam absorption, modest differences are difficult to discern.

Runs D and F show the respective differences between fueling the combustor with ethylene and methane (with ϕ held constant). Although not indicated by the figure, the peak instantaneous and average signal levels for methane were less than half that for ethylene. The structure of the average OH signal is very similar, with the bright region at the cowl-side wall indicative of the flame held there. Also, in both cases the fuel-rich plume near the body-side wall is evident from the absence of OH. However, the $\widehat{\sigma}$ images are much different. At the cowl-side wall, where there is little intermittency with ethylene, a large amount of intermittency exists with methane. This is also the case for the region in the top right of the images. This, of course, reflects the greater difficulty in burning methane in a scramjet combustor. Nonetheless, combustion efficiency, derived from thrust measurements, with methane fueling is surprisingly high, ~80%, and equal to that with ethylene.

3.2. Combustor pressure distributions

Figure 6 shows the measured combustor pressure distributions for several cases along with the duct geometry for reference. The plot presents the measured wall static pressure scaled by the mass flux of the air stream as a function of the normalized axial position x/H, where H is the height of the combustor flowpath at the engine throat location ($x/H = 0$). Each distribution contains measured static pressures from taps on the top, bottom, and both side walls. The data were time-averaged to some degree (pneumatic response through 6-foot long nylon pressure lines) and single time profiles of data taken at 1 Hz are shown. Pressure measurement uncertainty is approximately ±0.1% of reading.

Seven pressure distributions are shown in the plot. The tare measurements were obtained at the desired combustor operating conditions, but

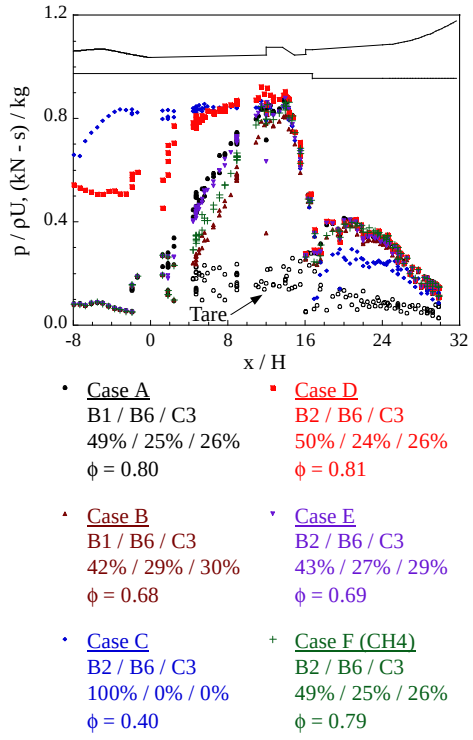

Fig. 6. Combustor pressure distributions. Measured wall pressure is scaled by the air stream mass flux and axial position is normalized by the combustor flowpath height at the engine throat location ($x/H = 0$). The flowpath is shown for reference. Details of the various combustion cases, including fuel type, fuel distribution, and overall ϕ, are shown.

with no fuel injection. This distribution serves as a reference for cases where fuel injection and combustion were present. Five combustion cases with ethylene and one with methane (see Table 1), are also represented in the plot. Cases A, C, D, and F have the same fuel mass flow rate from the primary injection site (either B1 or B2); cases B and E have 28% less fuel through the primary injectors while matching the flow rate through the secondary injectors to cases A and D. Cases A and D compare the operating characteristics associated with B1 and B2 injection for an overall equivalence ratio of $\phi = 0.8$. Both cases exhibit strong combustion in all of the flameholding regions as evidenced by the large pressure rises near $x/H = 12$ and $x/H = 20$. In case D, however, the pre-combustion pressure rise is observed to start at a position well upstream of $x/H = 0$. This condition, commonly called unstart because the shock train that is generated as a result of the pressure rise is positioned upstream of the engine throat, arises as a result of too much heat release in the region near the cavity flameholder. Based on this observation, it appears that B2 injection at these conditions produces slightly improved mixing and combustion compared with B1 injection. In these two cases, the pressure measurements downstream of the cavity flameholder are nearly indistinguishable from one another. This suggests that the top and bottom wall-step flameholders are relatively insensitive to the differences associated with the upstream injectors. The OH PLIF images taken downstream of the steps support this observation in that they show only slight differences between the two injection schemes.

The pressure measurements downstream of the step flameholders for cases B and E are indistinguishable from cases A and D. This further supports the observation that these step flameholders are insensitive to differences in upstream injection. For case B, the pressures upstream of the cavity flameholder are lower than in case A, which is consistent with lower fuel flow rate in that region. Also, with the lower upstream fuel injection for case E, unstart is not observed as it was in case D, and the pressures upstream of the cavity are similar to those in case A where the fuel flow rate is higher and the injection angle is lower.

For the case with B2-only injection (case C), an unstarted condition is again observed. The pressure data in the primary flameholding region compare very closely with the previous ethylene-injection case using B2. Here, however, the pressure rise associated with the downstream flameholding region is substantially suppressed compared with either of the previous cases. This shows the effectiveness of fueling the downstream region using both B6 and C3 injection sites, and the unstart phenomenon's lack of dependence on fueling from these sites. The reduction in pressure rise downstream of the flameholding steps suggests that a large portion of OH fluorescence signal for this case is a result of combustion products convected into the laser sheet.

Finally, one can compare the characteristics of the pressure distribution from case F with the one resulting from case D. In these two cases, the fuel distributions and overall values of ϕ are essentially identical. The pressure distributions reveal the influence of fuel reactivity on combustor operation. Methane injection results in a weakening of the primary combustion zone, as suggested by the downstream shift in the position of the pre-combustion pressure rise (in fact, the pressure rise in the methane case also begins downstream of that associated with ethylene injection using B1). There is also a slight decrease in the measured pressures near the step flameholders (near $x/H = 18$) that is probably a result of decreased reactivity of methane relative to ethylene. This is supported by the OH imaging where the OH is more intermittent behind these flameholding regions with methane fueling.

3.3. Combustor performance

Figure 7 shows combustion efficiency derived from the thrust measurements. A combustor performance code solves the 1D mass, momentum, and energy conservation equations, along with the state equation using measurements of reactant properties (temperatures and mass flow rates), load-cell force, heat loss, and ambient, base, and exit pressures. Four unknowns remain at the combustor exit: density, enthalpy, velocity, and mass fraction of unburned fuel. Velocity is determined directly from the momentum conservation equation. This allows the density and enthalpy to be determined directly from the mass and energy conservation equations, respectively. Finally, the mass fraction of unburned fuel (Y_F) is iteratively determined using a chemical equilibrium package and the state equation, where Y_F is varied until the density from the state equation converges to the density determined from mass conservation. Combustion efficiency is computed as $1 - Y_F$. This in-house approach to calculating combustion efficiency is compared with established approaches in the community (RJPA and GASL-1D) by Donbar et al. [22] and is shown to be in excellent agreement.

Results are presented for ethylene and methane combustion cases, including runs not shown with the OH images and pressure traces. Uncertainty in combustion efficiency is ±4% of reading (e.g., $\varepsilon_c = 0.80 \pm 0.03$). In cases with ethylene fueling, fuel injected from the primary site (B1 or B2) was $\phi_{primary} = 0.3$ (recall that higher fueling rates from B2 can unstart the combustor). The remaining fuel ($\phi - \phi_{primary}$) was delivered to the B6 and C3 injection sites in equal proportions. Combustion performance is observed to vary somewhat with overall ϕ for the ethylene cases, with increasing values of combustion efficiency being obtained at lower values of overall ϕ. Cases using B2 as the primary fuel injection site typically outperform those using B1 as the primary injection site by about 3% points, except for the lowest overall ϕ where the results are nearly identical. This observation is consistent with the pressure distributions shown in Fig. 6, where B2 injection appears to produce better mixing and combustion in the primary flameholding region.

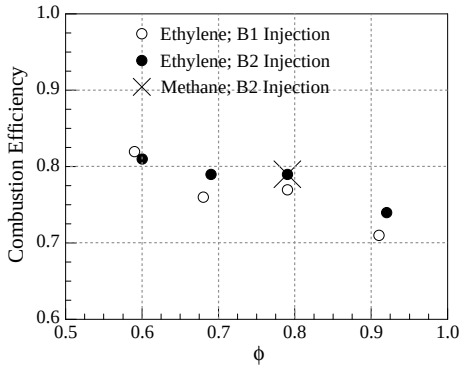

Fig. 7. Combustor performance. Combustion efficiency is shown as a function of overall ϕ with fuel (ethylene vs. methane) and primary fuel injection site (B1 or B2) as variables. Note that for each ethylene case, the ϕ from the primary fuel injection site was held constant at 0.3 and the balance of the fuel was split equally between B6 and C3. For the methane case, the primary fuel injection site had $\phi = 0.4$ with the balance again split equally between B6 and C3.

One case from methane injection is shown for comparison. Here, the overall ϕ was ~0.8, but the amount of fuel injected from the primary injection site (B2) was slightly higher ($\phi_{primary} = 0.4$) than with the ethylene cases ($\phi_{primary} = 0.3$). Combustion performance was found to compare favorably with the ethylene results. So, while the flameholding appears better with ethylene vs. methane (from both OH distributions and wall pressures), flameholding is still sufficient with methane to produce equivalent combustor performance for this combustor under the tested conditions.

4. Conclusions

1. The individual OH PLIF images indicate the flame front in the supersonic combustor is extremely dynamic in nature.
2. In cases where fuel is also injected on the cowl side, the cowl-side step performs well in anchoring the flame. Ethylene shows better flameholding characteristics than does methane, probably because of ethylene's greater reactivity.
3. Average planar laser-induced fluorescence images of OH show that 12 cm downstream of the B6 injectors, a high fuel concentration region is still visible behind the injectors. This indicates that fuel is still mixing well past the flameholding step.
4. Normal injection (B2) shows slightly better performance than injection at an angle of 30° (B1).
5. Fueling downstream of the main flameholding cavity (B6 and C3) creates higher pressures at the combustor exit, and thus yields better combustor performance, and does not lead to combustor unstart.
6. While most of the data are with ethylene fueling, the combustor was run with heated methane. In general similar burning patterns were observed in the PLIF images with methane vs. ethylene fueling. The only significant differences observed were that the pressure rise in the cavity region was delayed and the cowl flameholding was less stable in the case of methane fueling.

7. Combustion efficiency decreases slightly with increasing equivalence ratio, from ~82% at $\phi = 0.6$ to ~72% at $\phi = 0.9$; combustion efficiency with methane fueling compares favorably with that using ethylene (~80%) for the one condition tested.

Acknowledgments

This work was supported by the Advanced Propulsion Technology Program under the guidance of Robert Mercier and by the Air Force Office of Scientific Research under the guidance of Julian Tishkoff. The authors acknowledge the technical contributions of Stephen Smith of AFRL/RZA and Charles Smith, William Haendiges, Richard Ryman, and Jacob Diemer of Innovative Scientific Solutions, Inc. The support of the AFRL/RZ Research Air Facility is also appreciated.

References

[1] S. Rocci-Denis, D. Maier, W. Erhard, H. Kau, Free Stream Investigations on Methane Combustion in a Supersonic Air Flow, AIAA Paper 2005-3314, 2005.
[2] S. Tomioka, K. Kobayashi, K. Kudo, A. Murakami, T. Mitani, *J. Propul. Power* 19 (5) (2003) 876–884.
[3] S. Tomioka, K. Kobayashi, K. Kudo, A. Murakami, *J. Propul. Power* 21 (4) (2005) 760–762.
[4] X.J. Fan, G. Yu, J.G. Li, X.N. Lu, C.J. Sung, Performance of Supersonic Model Combustors with Distributed Injection of Supercritical Kerosene, AIAA Paper 2007-5406, July 2007.
[5] K. Yu, K.J. Wilson, K.C. Schadow, *J. Propul. Power* 17 (2001) 1287–1295.
[6] K. Yu, K.J. Wilson, R.A. Smith, K.C. Shadow, Experimental Investigation on Dual-Purpose Cavity in Supersonic Reacting Flows, AIAA Paper 1998-0723.
[7] A. Ben-Yakar, R.K. Hanson, *J. Propul. Power* 17 (4) (2001) 869–876.
[8] M.R. Gruber, J.M. Donbar, C.D. Carter, K.-Y. Hsu, *J. Propul. Power* 20 (5) (2004) 769–778.
[9] M.B. Colket, L.J. Spadaccini, *J. Propul. Power* 17 (2) (2001) 315–323.
[10] G.L. Pellett, S.N. Vaden, L.G. Wilson, Opposed Jet Burner Extinction Limits: Simple Mixed Hydrocarbon Scramjet Fuels vs. Air, AIAA Paper 2007-5664, July 2007.
[11] A. Paull, R.J. Stalker, D.J. Mee, *J. Fluid Mech.* 296 (1995) 159–183.
[12] L. Serre, ONERA Potential for Scramjet Ground Testing up to Mach 12, AIAA Paper 2005-3330, 2005.
[13] R.S. Barlow, R.W. Dibble, J.-Y. Chen, R.P. Lucht, *Combust. Flame* 82 (1990) 235–251.
[14] J.M. Donbar, M.R. Gruber, T.A. Jackson, C.D. Carter, T. Mathur, *Proc. Combust. Inst.* 28 (2000) 679–687.
[15] A. Bresson, P. Bouchardy, P. Magre, F. Grisch, OH/Acetone PLIF and CARS Thermometry in a Supersonic Reactive Layer, AIAA Paper 2001-1759, 2001.
[16] A. Ben-Yakar, R.K. Hanson, Hypervelocity Combustion Studies Using Simultaneous OH-PLIF and Schlieren Imaging in an Expansion Tube, AIAA Paper 99-2453, June 1999.
[17] C.C. Rasmussen, S.K. Dhanuka, J.F. Driscoll, *Proc. Combust. Inst.* 31 (2007) 2505–2512.
[18] R.A. Baurle, T. Mathur, M.R. Gruber, K.R. Jackson, A Numerical and Experimental Investigation of a Scramjet Combustor for Hypersonic Missile Applications, AIAA Paper 1998-3121, July 1998.
[19] T. Mathur, G. Streby, M. Gruber et al., Supersonic Combustion Experiments with a Cavity-Based Fuel Injector, AIAA Paper 1999-2102, June 1999.
[20] M. Gruber, K. Jackson, T. Mathur, F. Billig, Experiments with a Cavity-Based Fuel Injector for Scramjet Applications, ISABE Paper IS-7154, September 1999.
[21] M. Gruber, M. Hagenmaier, T. Mathur, Simulating Inlet Distortion in a Direct-Connect Scramjet Combustor, AIAA Paper 2006-4680, July 2006.
[22] J. Donbar, O. Powell, M. Gruber, T. Jackson, D. Eklund, T. Mathur, Post-Test Analysis of Flush-Wall Fuel Injection Experiments in a Scramjet, AIAA Paper 2001-3197, July 2001.